Critical Behavior in Monoclinic Cr_3Te_4

Anirban Goswami[1], Nicholas Ng[2,3], Emmanuel Yakubu[1], AM Milinda Abeykoon[4], and Samaresh Guchhait[1*]

1. Department of Physics and Astronomy, Howard University, Washington, DC 20059, USA
2. Department of Chemistry, The Johns Hopkins University, Baltimore, MD 21218, USA
3. Institute for Quantum Matter, The William H. Miller III Department of Physics and Astronomy, The Johns Hopkins University, Baltimore, MD 21218, USA
4. National Synchrotron Light Source-II, Brookhaven National Laboratory, Upton, NY 11733, USA

Abstract

High-quality monoclinic Cr_3Te_4 crystals are synthesized by the chemical vapor transport method and confirmed by synchrotron powder x-ray diffraction. Critical behaviors of Cr_3Te_4 are studied by bulk isothermal magnetization measurements around its paramagnetic-to-ferromagnetic phase transition. From this data, we evaluate the modified Arrott plot, the Kouvel-Fisher plot, critical isotherms, and estimate critical exponents values of $\beta \sim 0.3827$, $\gamma \sim 1.2119$, $\delta \sim 4.16$, and the Curie temperature $T_C \approx 321$ K. After the scaling, the isothermal magnetization curves below and above the critical temperatures collapse into two independent universal branches which signifies the reliability of our critical exponent estimation. The estimated critical exponent values of Cr_3Te_4 do not match well with theoretically calculated values of any three-dimensional models.

I. Introduction

Magnetic materials are interesting for fundamental studies and have many applications. A macroscopic magnetic system consists of many atoms with complex interactions between them. Although these systems can be very complex, they also exhibit some remarkable simplifications. A 2nd order magnetic system undergoes a continuous magnetic phase transition with a correlation length that diverges at the phase transition. Consequently, thermodynamic properties of these systems in the vicinity of the magnetic phase transition are largely independent of microscopic details and the underlying interactions of its constituents. Instead, they may fall into one of a small number of different classes characterized by global features, such as system dimensionality, symmetries, etc. This phenomenon is called universality, which finds a simple explanation within the framework of renormalization group theory. Near a 2nd order magnetic phase transition, thermodynamic quantities such as heat capacity, magnetic susceptibility, magnetization, etc., exhibit power-law dependencies on parameters as a function of the distance away from the phase transition (e.g., $T - T_C$, the departure of the measurement temperature T from the phase transition temperature T_C). The extracted powers are known as critical exponents, and their magnitude can shed light on the nature of the phase transition. We investigate here the critical behaviors of monoclinic Cr_3Te_4 around its paramagnetic-to-ferromagnetic phase transition temperature.

In recent years, chromium telluride compounds have drawn significant interest due to their diverse magnetic properties [1–11]. Cr-Te binary phase diagram has several stable binary phases [9,11–13]. They have been found to have several magnetic binary phases with transition temperatures ranging from 180 K up to 321 K [7]. Reported stable binary phases include hexagonal CrTe [14], hexagonal $CrTe_2$ [15–17], trigonal Cr_2Te_3 [18–20], monoclinic Cr_3Te_4 [7,21,22], layered Cr_4Te_5 [23], hexagonal $Cr_{1-x}Te$ ($x < 0.1$) [7] and trigonal & monoclinic phases of Cr_5Te_8 [24–26]. Recent theoretical studies have predicted some layered, room temperature magnetic Cr_xTe_y phases [2,12]. However, the material of interest for this paper is monoclinic Cr_3Te_4. This is an interesting material because it may be useful for room temperature magnetocaloric applications.

There are alternating stacks of Cr-full and Cr-deficient layers along the *c*-axis in these compounds. Cr content plays a crucial role in determining their structural and magnetic properties. Interestingly, some research groups studied these Cr-Te compounds in the 1960s and 1970s. But these studies mostly focused on material synthesis, followed by bulk magnetic, heat capacity, and electrical transport studies, and some density functional theory (DFT) calculations [7,8,21,27–30]. However, in recent times there is a renewed interest in this class of binary phases. A recent theoretical calculation predicted 2D layered room-temperature ferromagnetic Cr_xTe_y phases [2,12]. Recently, there is also a report of an anomalous Hall effect in trigonal Cr_5Te_8 [31]. A recent analysis of critical exponents of Cr_4Te_5 revealed the three-dimensional Heisenberg-like spin coupling inside this material [23].

The monoclinic Cr_3Te_4 phase was studied in 1960s and 1970s [7,8,21]. Powder neutron diffraction pattern at 4.2 K shows presence of both ferro and anti-ferromagnetic peaks [28] . However, this study does not have many details about temperature dependence of these peaks. Magnetic measurements show the presence of two magnetic phase transitions: ~100 and 320 K, which was corroborated by heat capacity [32] and transport studies [7]. Moreover, band structure calculation [13], reflectivity spectra [33], and magneto-optical effect [34] studies are reported on Cr_3Te_4. However, these studies did not address the nature of magnetic phase transition in this material which will be addressed here.

To evaluate possible applications of this material, it is necessary to investigate the nature of its magnetic phase transition. In this work, we focus on understanding the nature of magnetic phase transition in Cr_3Te_4 crystals. First, we analyze its crystal structure by synchrotron powder x-ray diffraction. Then we investigate the critical behavior of Cr_3Te_4 by using modified Arrott plot, Kouvel-Fisher plot, and critical isothermal analysis. Previously, critical behavior analysis has been reported on other Cr-Te binary phases such as $Cr_{0.62}Te$ [26], $CrTe_2$ [15], Cr_4Te_5 [23], Cr_5Te_8 [24,25], etc. However, to best of our knowledge, this is the first time this kind of analysis of critical exponents is reported on Cr_3Te_4. Using the estimated critical exponents, we estimate the length scale of magnetic exchange interaction. Moreover, this may be a useful material for magnetocaloric applications which use entropy change at the magnetic phase transition to transfer

heat. The magnetocaloric effect is also related to the critical behaviors at magnetic phase transition [25,35–38]. The relative power cooling (RCP) and magnetic entropy change are two important parameters to characterize the usefulness of magnetocaloric materials. Both RCP and magnetic entropy changes at the transition have power law dependences on the applied magnetic field where these exponents are also functions of critical exponents [39–42]. Therefore, this study will be helpful to understand the usefulness of this material for practical applications.

II. Sample Synthesis and phase analysis

Cr_3Te_4 crystals were synthesized by chemical vapor transport (CVT) using Cr and Te elements, with I_2 as the transport agent. These CVT synthesis were performed in a Thermo Scientific Lindberg Blue M three-zone furnace equipped with UP150 model program controllers. Cr (Alfa Aesar, powder, -100+325 mesh, 99.99% metals basis) and Te (Thermo Scientific, shot, 2-5mm diameter, 99.9999% metals basis) were used as received without further purification. Between 35-50 mg of solid I_2 was used as the vapor transport agent. Stoichiometric amounts of Cr and Te plus the transport agent were placed inside a fused quartz tube and sealed under vacuum. The sealed tube was, at minimum, long enough to equal the distance between the centers of two zones of a three-zone furnace. This tube was then placed inside the three-zone furnace. All three zones were heated at a rate of 100 ^oC per hour, with the charge zone reaching 1050 ^oC and the crystallization zone reaching 820 ^oC. This temperature gradient was held for 7 days, then the furnace was cooled at a rate of 100 ^oC per hour to room temperature. Synthesized crystals of Cr_3Te_4 are silvery metallic in color and are generally between 1-5 mm in dimensions.

Room temperature x-ray powder diffraction measurements were carried out at the Pair Distribution Function (PDF) beamline 28-ID-1 of the National Synchrotron Light Source-II. Cr_3Te_4 crystals were grounded to get the powder sample. Data were collected in capillary transmission geometry using a PerkinElmer amorphous silicon detector placed 1000 mm downstream from the sample. The setup utilized a 74.5 keV (λ = 0.1665 $^{\circ}$A) X-ray beam. Two-dimensional diffraction data were radially integrated to obtain intensity vs Q data using the pyFAI software package [43]. The Rietveld refinement was carried out using the GSAS-II software package [44]. Figure 1(a) shows the powder X-ray diffraction pattern of Cr_3Te_4 sample, and the corresponding Rietveld fit. The inset of Figure 1 shows the refined crystal structure of monoclinic Cr_3Te_4 generated using CrysX-3D Viewer [45]. The powder diffraction pattern was fitted with the symmetry space group H-M "C 1 2/m 1". The refined unit cell parameters are a = 13.977(11), b = 3.930(0), c = 6.862(3), β = 118.281(11)^o. Refined fractional coordinates, occupancy of Cr and Te, and the isotropic thermal displacement parameters (Uiso) are given in Table I. The corresponding crystallographic information file (cif) is included as supplementary material (see the Supplementary Materials [46]). All parameters related to this refinement are included in Table II. The Laue diffraction is used to determine the crystallographic axes of the Cr_3Te_4 crystal using the crystal structural parameters obtained from the refinement, as shown in Figure 1(b).

Table I: Results of the Rietveld refinement.

Element	x	y	z	occupancy	Uiso (Å²)
Cr^{2+}	0.0000	0.0000	0.0000	0.904(4)	0.0102(9)
Cr^{3+}	0.2558(2)	0.0000	0.2732(3)	1.000	0.0080(4)
Te	0.3677(1)	0.0000	0.0305(1)	1.000	0.0069(2)
Te	0.1188(1)	0.0000	0.4531(1)	1.000	0.0078(2)

Table II: Various parameters related to the Rietveld refinement.

No of functions calls	5
No of observations	3080
No of parameters	30
wR	3.32%
χ^2	276.515
Reduced χ^2	0.09
Goodness-of-Fit (GOF)	0.30
RF	1.26%
RF^2 (on 543 reflections)	2.75%
Durbin-Watson statistics	0.091
Bragg intensity sum	1.67e+05
PWDR histogram weight factor	1.000
R	2.5%
R-bkg	2.53%
wR-bkg	3.32%
wR-min	11.08%

III. Magnetic Studies and Analysis of Critical Exponents

A Quantum Design Physical Property Measurement System (PPMS) 9 Tesla Dynacool model was used for all these magnetic studies. A Cr_3Te_4 crystal of 18.5 mg mass was used for all magnetic studies reported here. We studied 4 samples for the consistency check. Figure 2 shows the temperature-dependent zero-field-cooled (ZFC) and field-cooled (FC) magnetization (M) studies of the Cr_3Te_4 crystal at 1000 Oe magnetic field (H) applied along *ab*-plane and *c*-axis. For the ZFC study, the sample was rapidly cooled down to 2 K in zero field, then a 1000 Oe field was applied and the sample ZFC magnetic moment was measured with increasing temperature (T) up to 400 K. For the FC study, the sample was cooled down to 2 K in presence of the same field. The temperature dependent magnetization studies show two phase transitions: one at about 320 K and another below 100 K. While the high temperature phase transition appears to be from a paramagnetic to a ferromagnetic phase, the low temperature (below 100 K) phase transition seems to have some anti-ferromagnetic component. This agrees well with previous powder neutron

diffraction study [8]. This type of transition is also reported in Cr_4Te_5 [23] and Cr_5Te_8 [25,47], which is ascribed to the presence of a canted antiferromagnetic structure.

Figure 3 plots field dependence of magnetization for the Cr_3Te_4 crystal along (a) *c*-axis and (b) *ab*-plane for four different temperatures. For temperatures above 100 K, magnetization curves along the *c*-axis change rapidly with changing field within about ±1000 Oe field range, and then changes slowly with changing magnetic field outside this field range. However, field dependent magnetization curves along the *ab*-plane make this transition around ±1 Tesla field. This is an indication that above 100 K the magnetic easy axis is along the *c*-axis of Cr_3Te_4. But the 2 K magnetization curves for field along both directions make this transition around ±1 Tesla field. Previous powder neutron diffraction studies [8] have reported a rotation of magnetic easy axis direction below ~100 K temperature, which could explain our 2 K field dependent magnetization data. Moreover, a closer inspection of the 2 K magnetization curves for field show that magnetizations do not saturate even at ±9 Tesla magnetic field. Furthermore, we estimate an effective magnetic moment of ~2.65 μ_B per Cr atom at 9 T field at 2 K, which agrees well with other studies [5,29].

The isothermal magnetizations around the high-temperature paramagnetic-ferromagnetic phase transition region are used to study the critical behaviors of Cr_3Te_4. We measured magnetizations from 0 to 9 Tesla field for a constant temperature. Through the analysis of the isothermal magnetizations, we will be able to determine the critical exponents associated with this phase transition [49]. These isothermal magnetizations were done for a temperature range from 290 to 350 K with an increment of 2 K. Figure 4 is a plot of isothermal magnetizations along *c*-axis. The Arrott-Noaks equation of state [49] is given as

$$(H/M)^{1/\gamma} = a\,\varepsilon + b\,M^{1/\beta}, \qquad (1)$$

where $\varepsilon = (T - T_C)/T_C$ is the reduced temperature, T_C is the Curie temperature, and *a*, *b* are two constants. For appropriate β and γ values, the isothermal magnetization at $T = T_C$ will be a straight line passing through the origin. For the mean-field theory $\beta = 0.5$ and $\gamma = 1$ which gives rise to the (conventional) Arrott plot [50]. Figure 5 shows the Arrott plot (M^2 vs H/M) for Cr_3Te_4. It is known that the Arrott plot is a conventional method to determine the Curie temperature. In the high magnetic field region, the linear nature of the curves will signify the mean field type interaction. In the Arrott plot (Figure 5), all the curves show nonlinear behavior with a downward curvature in the high field region indicating a non-mean-field-like behavior. In addition to that, the concave (downward) nature of the curves strongly suggests a 2nd order magnetic phase transition, in accordance with the Banerjee's criterion [51]. This deviation from the mean field theory is expected because the mean field theory neglects the effects of spin fluctuations and correlation which are generally present in real magnetic materials.

Besides the mean-field model, there are other three-dimensional (3D) models with theoretically calculated β and γ values. To find out if the Cr_3Te_4 phase transition can be described by any of these 3D models, we plotted the modified Arrott plots using known β and γ values of these models (Figure 6). These known 3D models are: (a) tri-critical mean-field model (β=0.25, γ=1.0), (b) 3D Ising model (β=0.325, γ=1.24), (c) 3D XY model (β=0.345, γ=1.316), (d) 3D Heisenberg model (β= 0.365, γ=1.386) [51,52]. Using γ and β values from these models, we failed to generate parallel straight lines (in the high field region) suggesting that *none* these 3D models are best suited to describe the magnetic phase transition in this material.

It is well-known that the critical behavior of a 2nd order phase transition can be explained by a series of interrelated critical exponents. Near a second-order magnetic phase transition, the correlation length ξ diverges as

$$\xi = \xi_0 |(T - T_C)/T_C|^{-\nu} , \qquad (2)$$

where ν is a critical exponent. This leads to the universal scaling laws for the spontaneous magnetization M_S and the inverse initial magnetic susceptibility χ_0^{-1}. The set of critical exponents β, γ, and δ are determined by the temperature-dependences of spontaneous magnetization $M_S(T)$ below T_C, inverse initial magnetic susceptibility $\chi_0^{-1}(T)$ above T_C, and measured field-dependent magnetization M(H) at T_C, respectively. The corresponding mathematical expressions are the following:

$$M_s(T) = M_0(T)(-\epsilon)^{\beta}, \epsilon < 0, T < T_C, \qquad (3)$$

$$\chi_0^{-1}(T) = (h_0/m_0)(\epsilon)^{\gamma}, \epsilon > 0, T > T_C \qquad (4)$$

$$M = DH^{1/\delta}, \ \epsilon = 0, T = T_C \qquad (5)$$

where $\varepsilon = (T - T_C)/T_C$ is called the reduced temperature, and M_0, h_0/m_0, and D are called critical amplitudes [53].

Moreover, the magnetic equation of state is a relationship among the variables M (H, ε), H, and T. Using the scaling hypothesis, the magnetic equation of state can be expressed as

$$M(H, \varepsilon) = \varepsilon^{\beta} f_{\pm}(H/\varepsilon^{\beta+\gamma}), \qquad (6)$$

where f_+ for $T>T_C$ and f_- for $T<T_C$, are two regular functions. In terms of renormalized magnetization $m \equiv \varepsilon^{-\beta} M(H, \varepsilon)$ and renormalized field $h \equiv \varepsilon^{-(\beta+\gamma)} H$, equation (6) can be written as

$$m = f_{\pm}(h), \qquad (7)$$

which signifies that for correct values of critical exponents (β, γ, and δ) and Curie temperature (T_C), scaled m and h will overlap on two universal curves: one above T_C and another below T_C. This is an important verification criterion for our analysis of critical exponents [53].

Because the conventional Arrott plot (Figure 5) did not generate parallel straight lines in high-field region, we need to estimate critical exponent values for Cr_3Te_4 magnetic phase transition. We used an iterative method to find the β, γ, and T_C values for Cr_3Te_4 as described by Pramanik and Banerjee [54]. Starting with the (conventional) Arrott plot, we estimate spontaneous magnetization (M_S) for temperatures below T_C and the inverse of initial magnetic susceptibility (χ_0^{-1}) for temperatures above T_C by extrapolating the linear portion of the curves (in high magnetic field region) to y-axis and x-axis, respectively. After plotting these estimated $M_S(T)$ and $\chi_0^{-1}(T)$ values for different temperatures, we determine a new set of β and γ values by fitting these data with the equations (3) & (4), respectively. Using these new set of values of β, γ, and T_C, we plot a modified Arrott plot (MAP) and repeat the above-mentioned steps until β, γ, and T_C reach respective stationary values. The estimated stationary values of critical exponents are β = 0.3814(±0.0046) and γ = 1.2243±0.0036. The final modified Arrott plots generated with these β and γ values is shown in Figure 7. A set of parallel straight lines in the high-field region demonstrates the validity of our β and γ estimation. The corresponding plots of $M_S(T)$ and $\chi_0^{-1}(T)$ are shown in Figure 8. By fitting these data sets to Eqs. (3) and (4), we estimate T_C = 320.51±0.077 and 321.07±0.043 K, respectively. The estimated critical exponent values by this iterative method are independent of their starting values which implies that the estimated critical exponents are reliable and correct.

Alternatively, the critical exponents β and γ can be determined by the Kouvel-Fisher (KF) method [55]. According to Kouvel and Fisher, following relations hold for a 2nd order magnetic phase transition:

$$\frac{M_S(T)}{\frac{dM_S(T)}{dT}} = \frac{T-T_C}{\beta} \qquad (8)$$

$$\frac{1/\chi_0(T)}{\frac{d(1/\chi_0)(T)}{dT}} = \frac{T-T_C}{\gamma} \qquad (9)$$

By analyzing the final modified Arrott plot's $M_S(T)$ data using Eq. (8) and $\chi_0^{-1}(T)$ data using Eq. (9), we get β = 0.3827±0.0035 with T_C = 320.97±0.051 K and γ = 1.2119±0.0063 with T_C = 321.17±0.071 K, respectively (Figure 9). The estimated β, γ, & T_C values from the Kouvel-Fisher method are consistent with those estimated from the final modified Arrott plot (MAP). This is another verification of reliability of our estimated critical exponents. Moreover, according to equation (5), the isothermal magnetization M(H) at T_C should be a straight-line with a slope of 1/δ in the logarithmic scale. From the measured M(H) curve at T_C, we estimate δ = 4.140 ±0.002 (Figure 10). Additionally, we can calculate δ value using the Widom scaling law [56]: $\delta = 1 + \frac{\gamma}{\beta}$. Using the estimated β and γ values from the final modified Arrott plot and the Kouvel-Fisher plot, we calculate δ = 4.21 and 4.16, respectively. These δ values agree well with one obtained from critical isotherm analysis. Therefore, three critical exponents β, γ, δ, and Curie temperature T_C estimated in this study are self-consistent and accurate within our experimental limitations.

The reliability of the estimated critical exponents and Curie temperature has been further verified by scaling analysis. In Figure 11(a), we plot the scaled magnetization (m) as a function of scaled magnetic field (h) in a linear scale. All the data collapse onto two separate branches below and above T_C, which is consistent with the scaling equation (7). This has also been verified in the plot of m^2 vs. h/m in Figure 11(b), where all data collapse onto two different branches like previous one, indicating the proper values of estimated critical exponents. The scaling equation of state has another form:

$$\frac{H}{M^{\delta}} = k\left(\frac{\varepsilon}{H^{1/\beta}}\right), \qquad (10)$$

where $k(x)$ is the scaling function. According to Eq. (10), all the experimental data will fall into a single universal curve when they are scaled accurately. This is shown in Figure 11(c), a plot of $MH^{-1/\delta}$ vs. $\varepsilon H^{-1/(\beta\delta)}$ where all isothermal magnetization data collapse into a single universal curve and T_C is at the zero point of the horizontal axis. This is another confirmation of the reliability of our estimated critical exponents.

For a comparison, our estimated critical exponents and those calculated from different theoretical models are summarized in Table III. According to the estimated critical exponents, Cr_3Te_4 can't be categorized in any single universality class. The value of exponent β lies between the 3D Heisenberg model and mean field model values. However, β value of Cr_3Te_4 is much closer to the value of the 3D Heisenberg model, which implies the existence of long-range ordered exchange interaction. Moreover, γ value lies between the 3D Ising model and mean-field model values, which points to the presence of strong uniaxial magnetic anisotropy in Cr_3Te_4 as shown in Figures 2 and 3. The presence of multiple interactions in this system may well explain this discrepancy of critical exponent values between our estimation and known theoretical models, which are based on simple magnetic interaction between spins.

We also can estimate the effective magnetic moment per Cr atom in the paramagnetic phase of Cr_3Te_4 by analyzing the temperature dependent magnetic susceptibility and inverse initial magnetic susceptibility data (Figure 12). Temperature-dependent magnetic susceptibilities are calculated from the temperature-dependent magnetization data, as shown in Figure 2. Also, we can calculate temperature-dependent initial magnetic susceptibility by analyzing the isothermal magnetizations above T_C (Figure 8). By the fitting these data to the Curie-Weiss law, we get the effective magnetic moment per Cr atom in the paramagnetic phase and Curie-Weiss temperature. Our estimated magnetic moments per Cr atom in the paramagnetic phase are 3.624±0.007 μ_B, 3.541±0.005 μ_B, and 3.994±0.009 μ_B for H || *c*-axis, H || *ab*-plane, and χ_0^{-1} plots, respectively. These values agree with other studies [5,43]. For a comparison, the theoretical values of expected magnetic moment of Cr^{2+} and Cr^{3+} ions are 2.83 μ_B and 3.87 μ_B, respectively. Moreover, our estimated empirical Curie-Weiss temperatures are +328.24±0.33, +325.68±0.16 and +327.65±0.25 K for H || *c*-axis, H || *ab*-plane, and χ_0^{-1} plots, respectively. These empirical Curie-

Weiss temperatures are slightly higher than the Curie temperature estimated by the analysis of critical exponents.

Additionally, it is important to analyze the nature of the magnetic interaction range in Cr_3Te_4. It is known that the universality class of magnetic phase transition depends on the range of the exchange interaction J(r). According to the renormalization group theory, the interaction decays with distance *r* as the following,

$$J(r) \approx r^{-(d+\sigma)} \quad , \qquad (11)$$

where σ is a positive constant and *d* is the system dimensionality. Moreover, the susceptibility critical exponent γ can be expressed as

$$\gamma = 1 + \frac{4}{d}\left(\frac{n+2}{n+8}\right)\Delta\sigma + \frac{8(n+2)(n-4)}{d^2(n+8)^2} \times \left[1 + \frac{2G\left(d/2\right)(7n+20)}{(n-4)(n+8)}\right]\Delta\sigma^2 \quad (12)$$

where $\Delta\sigma = \left(\sigma - \frac{d}{2}\right)$, $G\left(\frac{d}{2}\right) = 3 - \frac{1}{4}\left(\frac{d}{2}\right)^2$, and *n* is the spin dimensionality [57, 58]. Our estimated critical exponents do not exactly match any theoretical model. So, we will use various combinations of *d* and *n* to estimate σ using Eq. 12. Moreover, to check the consistency of our assumption, we will calculate these critical exponents using the following equations in succession: $\nu = \gamma/\sigma$, $\alpha = 2-\nu d$, $\beta = (2-\alpha-\gamma)/2$, and $\delta = 1+\gamma/\beta$. Here ν and α are the critical exponents of correlation length and heat capacity, respectively. Our estimated critical exponents are close to 3D Heisenberg model values (Table III). So, it is natural to use $d = 3$ and $n = 3$ first, which gives us $\sigma = 1.78$ using Eq. 12. Furthermore, the self-consistency check gives us $\beta = 0.4046$, $\gamma = 1.1856$, and $\delta = 3.91$, which are in good agreement with our estimated critical exponent values (Table III). All other combinations of *d* and *n* (such as 3:2, 3:1, 2:3, etc.) fail this self-consistency check. For a Heisenberg-type system in a 3D isotropic magnet, $\sigma > 2$ and $J(r)$ decreases faster than r^{-5}. When $\sigma \leq 3/2$, the mean field model more accurately describes the system, and J(r) decreases slower than $r^{-4.5}$. In the present case, it is found that the magnetic exchange distance decays as $J(r) \approx r^{-4.78}$, which lies between that of the 3D Heisenberg model and mean-field model.

IV. **Conclusion**

In summary, we have grown Cr_3Te_4 crystals by chemical vapor transport (CVT) method. We studied the crystal structure of Cr_3Te_4 by XRD methods. We made a comprehensive study of its critical behavior at its paramagnetic-ferromagnetic phase transition at ~321 K, which can be described as a 2nd order magnetic phase transition. By analyzing the isothermal magnetizations around the magnetic phase transition temperature, we estimated critical exponents $\beta \approx 0.3827$, $\gamma \approx 1.2119$, $\delta \approx 4.14$, and the Curie temperature $T_C \approx 321$ K by the modified Arrott plot and Kouvel-

Fisher method. Next, we use the scaling analysis to check the reliability of our critical value estimations. Our estimated Cr_3Te_4 critical exponents do not match with theoretically calculated values of any known 3D models. Moreover, we estimate the magnetic exchange distance in Cr_3Te_4 which decays as $r^{-4.78}$. Our study shows that Cr_3Te_4 has a large uniaxial magnetic anisotropy which may be useful for novel spintronic applications. Furthermore, our analysis of critical exponents will be useful to understand its magnetocaloric effects.

Acknowledgements

This work is supported by the National Science Foundation Awards No. DMR-2018579 and No. DMR-2302436. This work made use of the synthesis facility of the Platform for the Accelerated Realization, Analysis, and Discovery of Interface Materials (PARADIM), which is supported by the National Science Foundation under Cooperative Agreement No. DMR-2039380. This research used beamline 28-ID-1 of the National Synchrotron Light Source-II, a U.S. Department of Energy (DOE) Office of Science User Facility operated for the DOE Office of Science by Brookhaven National Laboratory under Contract No. DE-SC0012704. The authors are grateful to Prof. Raymond Orbach of the University of Texas at Austin and Dr. John Tranquada of Brookhaven National Laboratory for thoughtful discussions.

*Address of correspondence: samaresh.guchhait@Howard.edu

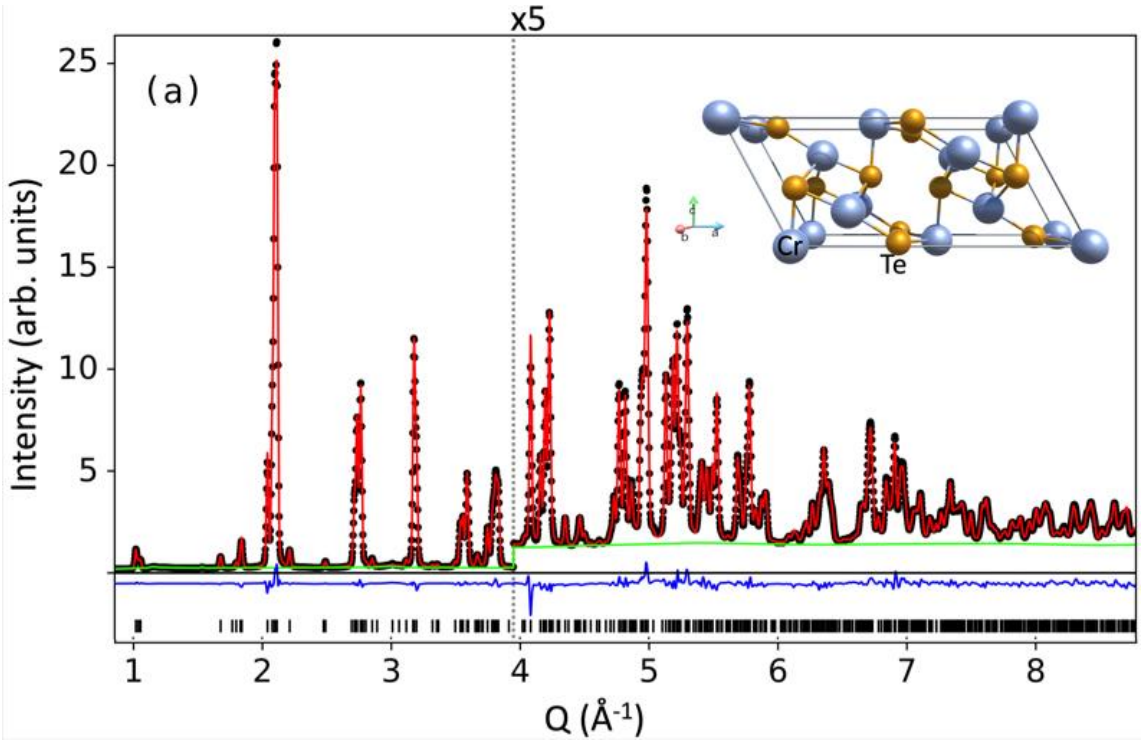

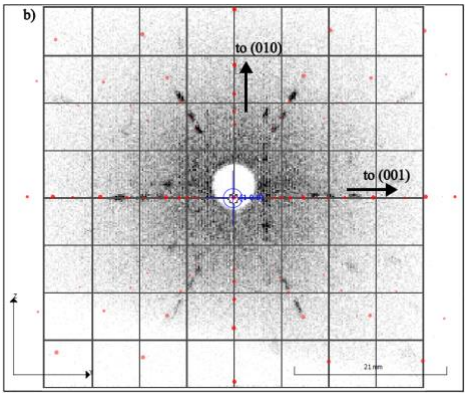

Figure 1: (a) Rietveld fit to room temperature powder diffraction data. Black dots and the red line represent measured and calculated intensities, respectively. The green line represents the polynomial fit to the background that was subtracted in the Rietveld refinement. A residue plot (blue), and calculated Bragg reflection tick marks are shown below. The observed and calculated intensities, and the fit residue above Q = 3.9 $Å^{-1}$ are multiplied by 5 for clarity. The inset shows Cr_3Te_4 crystal structure in 3-dimensional form, plotted using VESTA software after the refinement. (b) Laue diffraction image of the Cr_3Te_4 crystal. The sample is oriented along the crystallographic (100) axis. Arrows show the direction to the other crystallographic axes, as simulated by the QLaue software.

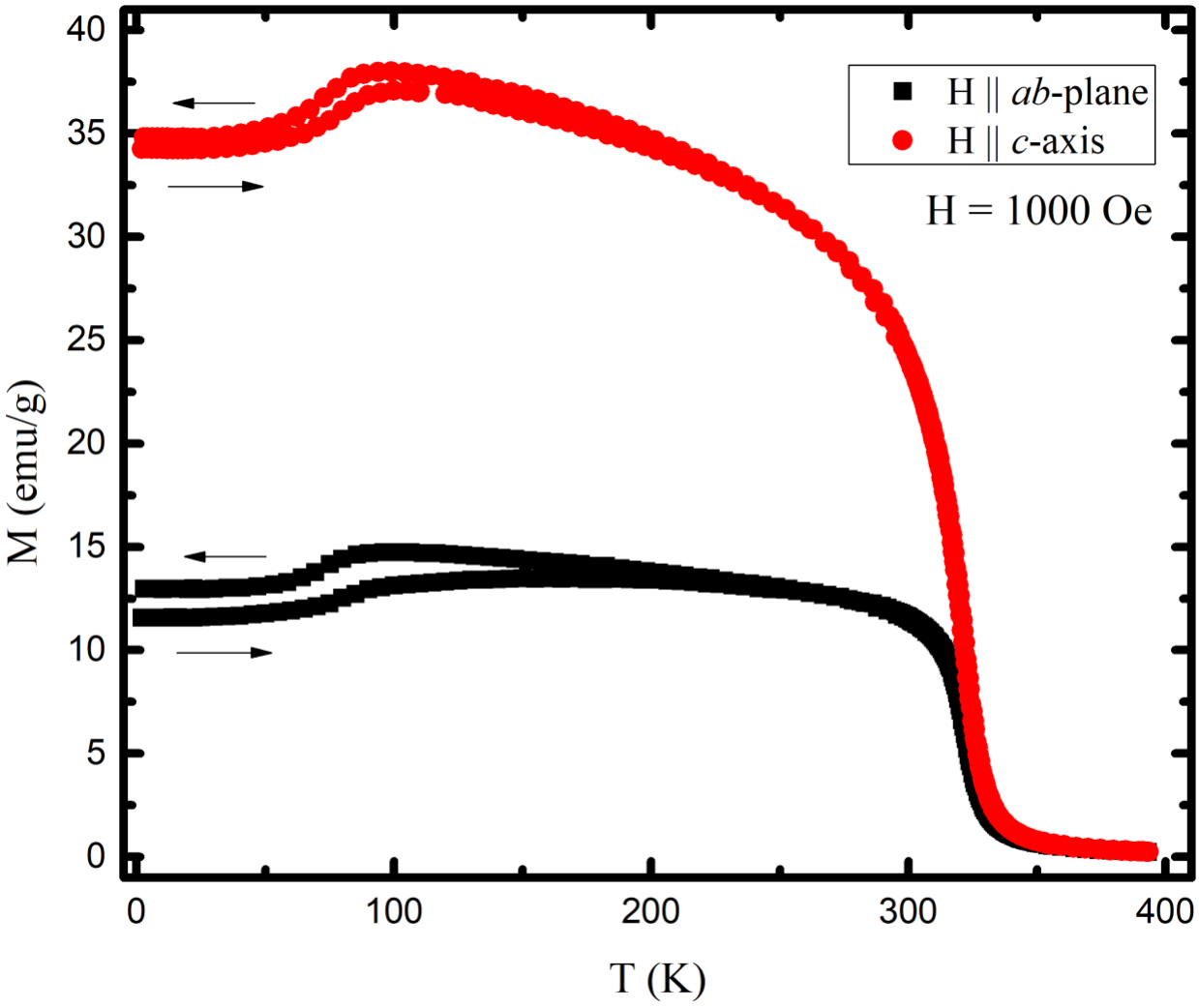

Figure 2: Temperature (T) dependence of field-cooled and zero-field-cooled magnetizations (M) measured along the *c*-axis and *ab*-plane of the Cr_3Te_4 crystal. This figure indicates presence of two magnetic phase transitions in Cr_3Te_4: a high-temperature transition around 320 K and another transition below 100 K.

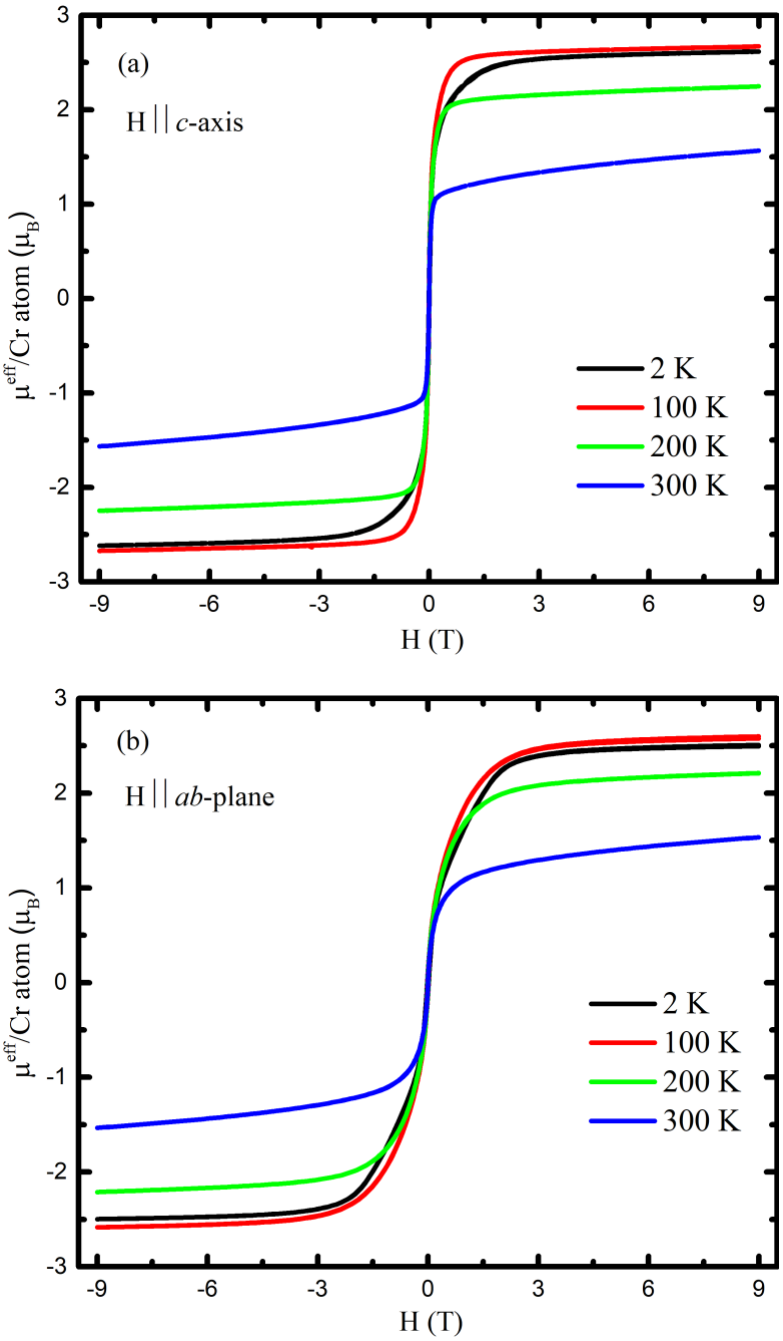

Figure 3: Temperatures-dependent magnetization curves for field of the Cr_3Te_4 crystal performed along (a) *c*-axis and (b) *ab*-plane.

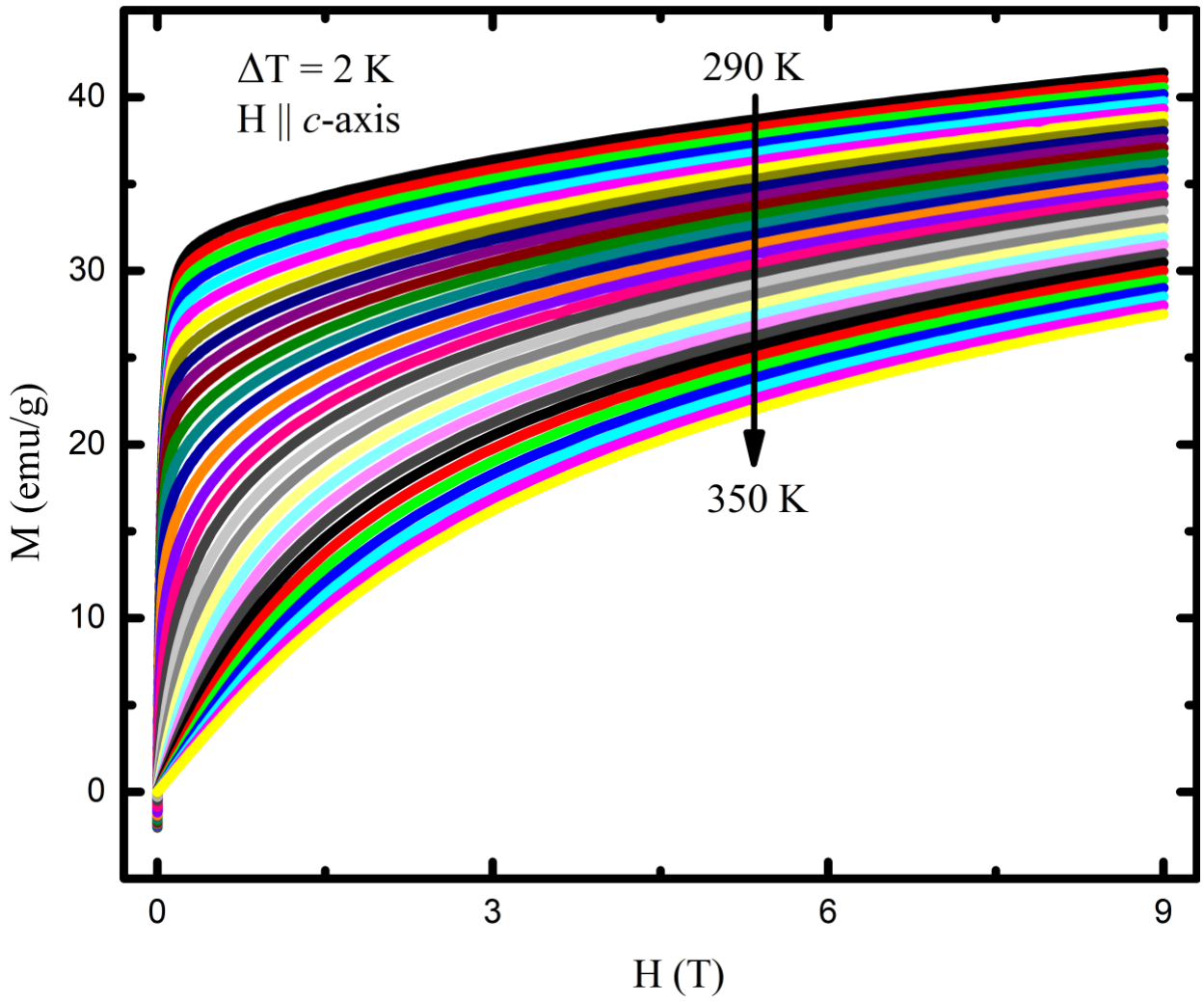

Figure 4: The isothermal magnetization measured along the *c*-axis at 2 K interval around the high-temperature magnetic phase transition for the Cr_3Te_4 sample.

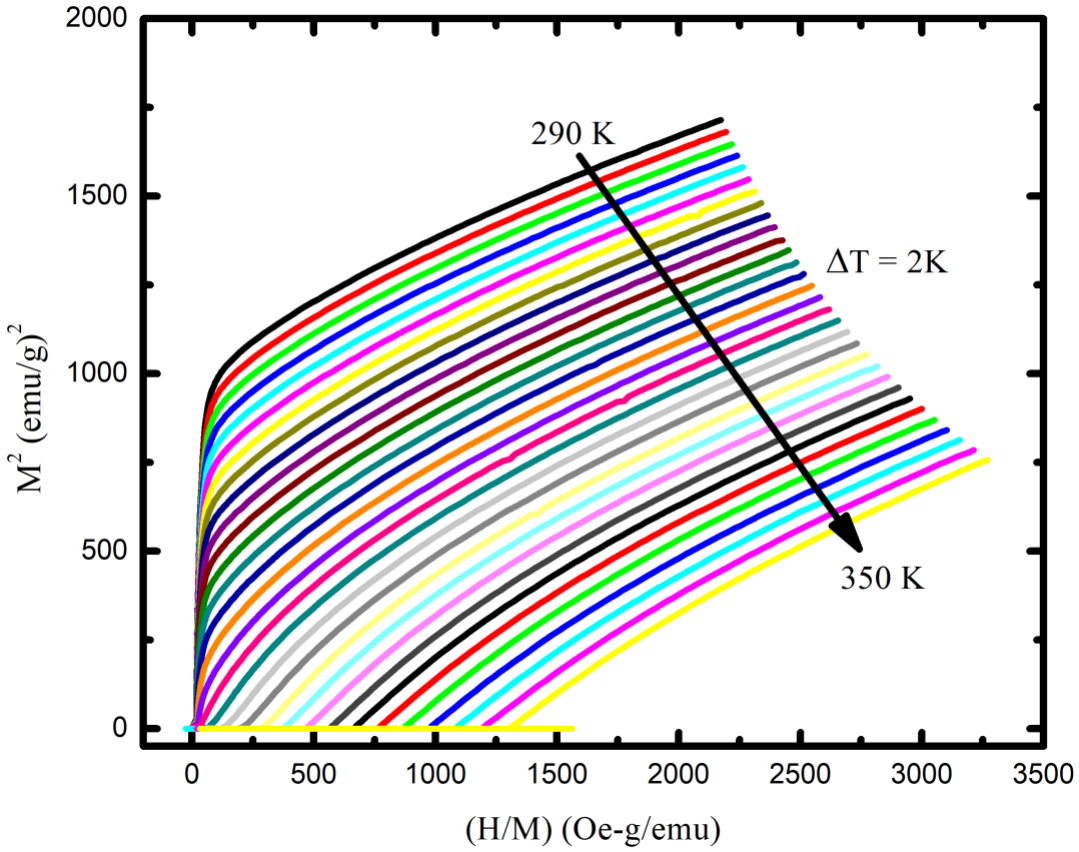

Figure 5: The Arrott plot of isothermal magnetizations along the *c*-axis of the Cr_3Te_4 crystal shows clear deviation from the mean-field model description of Cr_3Te_4 magnetic phase transition.

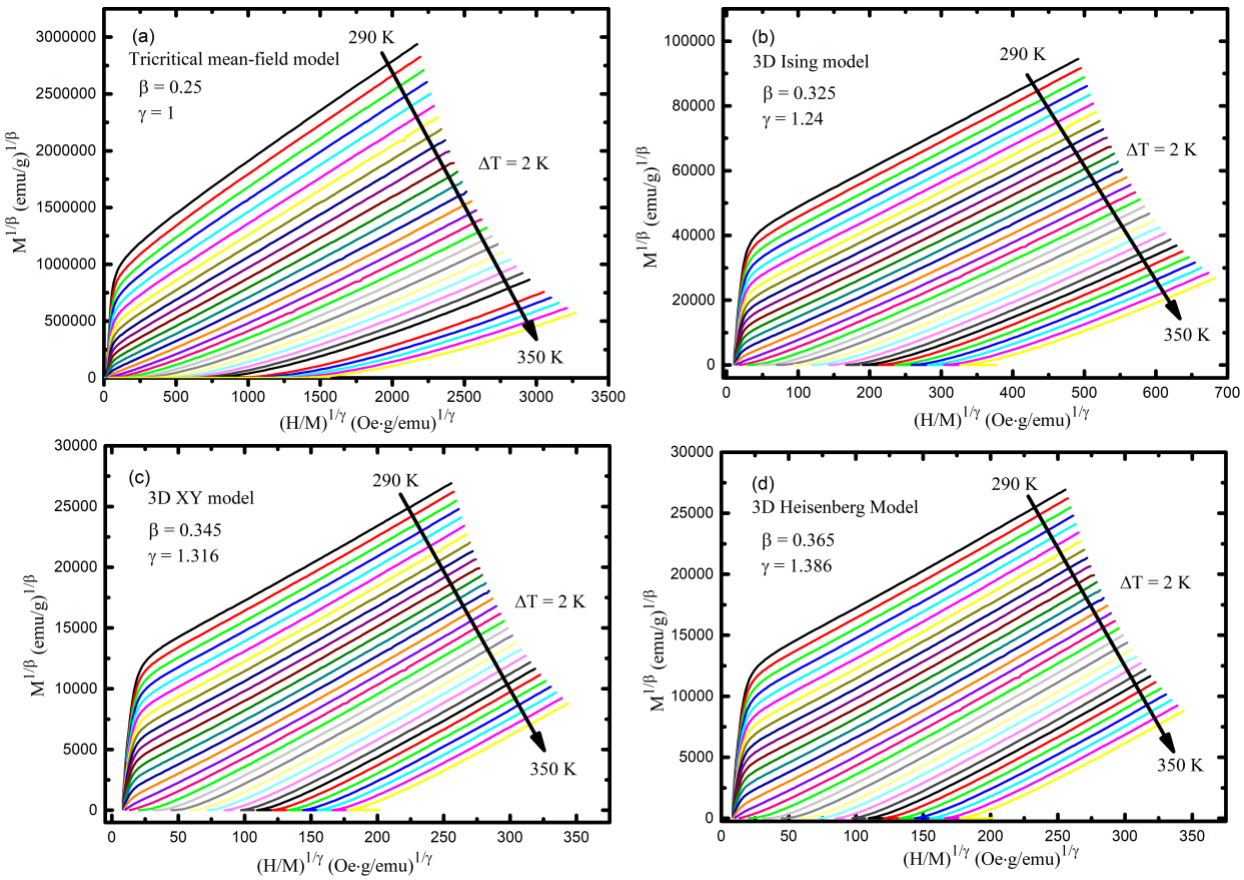

Figure 6: Modified Arrott plots of isothermal magnetizations plotted using known β and γ values from four models: (a) tri-critical mean field model, (b) 3D Ising model, (c) 3D XY model, and (d) 3D Heisenberg model. In the high field limits, isothermal magnetizations of these plots are not parallel to each other, indicating that any of these four models may not be most effective in describing the critical behaviors at Cr_3Te_4 magnetic phase transition.

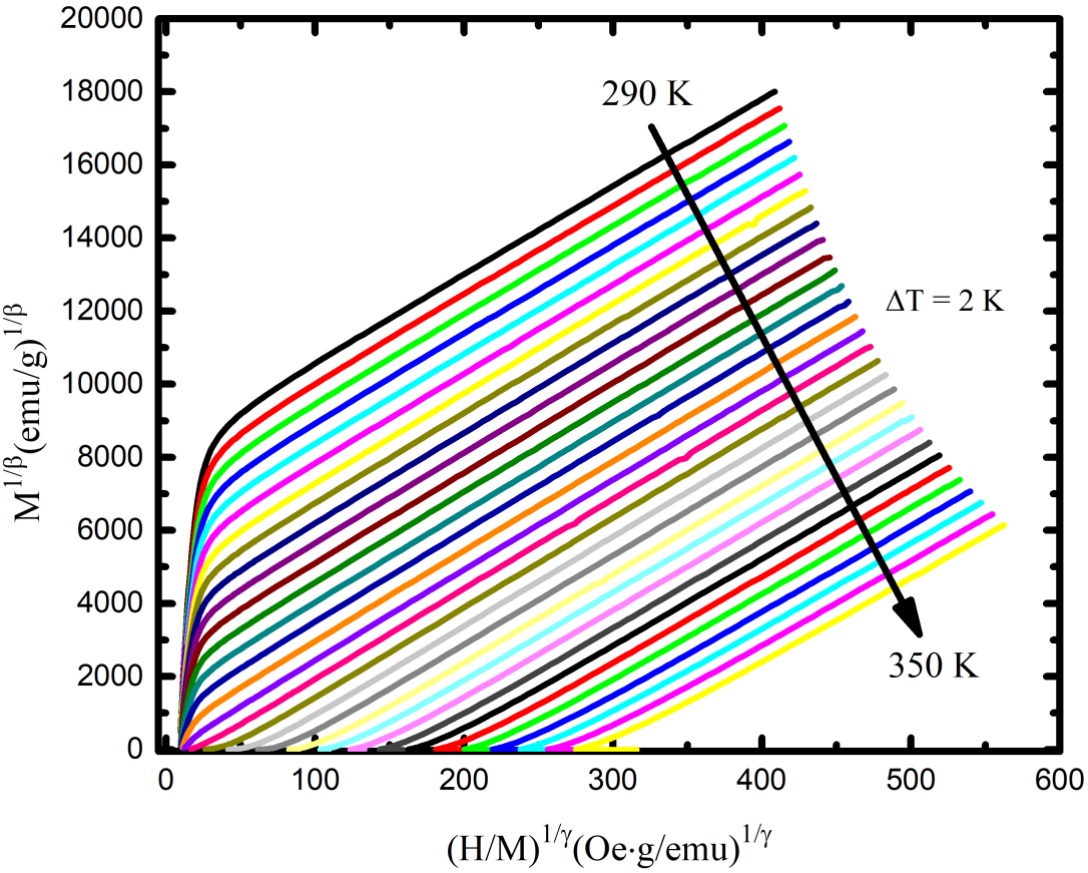

Figure 7: The modified Arrott plot of the isothermal magnetizations around the magnetic phase transition temperature plotted with the optimum fitted values of $\beta = 0.3814$ and $\gamma = 1.2215$.

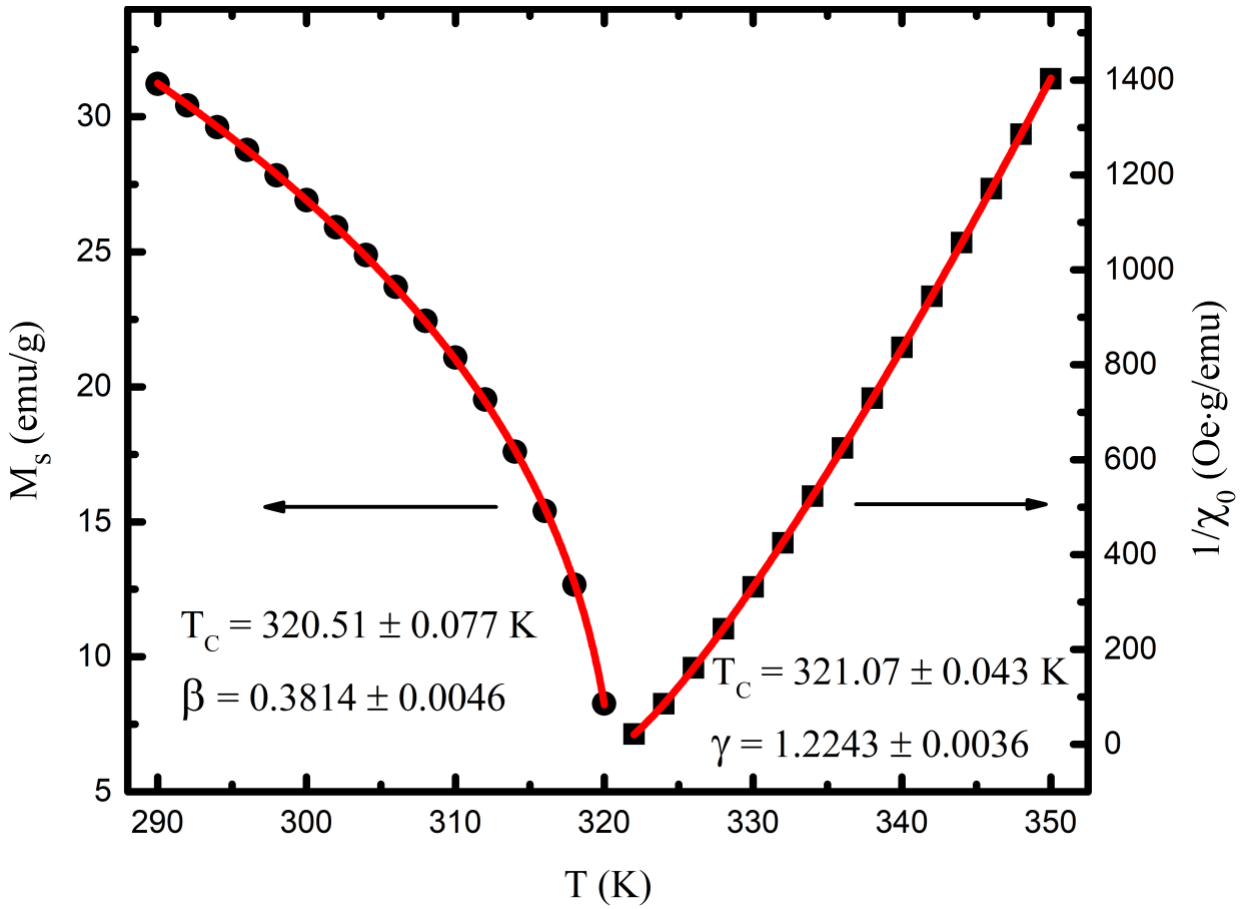

Figure 8: Temperature dependent spontaneous magnetization (M_S) and inverse initial susceptibility (χ_0^{-1}) are plotted around the magnetic phase transition. M_S and χ_0^{-1} are extracted by extrapolating the modified Arrott plot at high field regions. Estimated β, γ, and T_C values are shown in the figure.

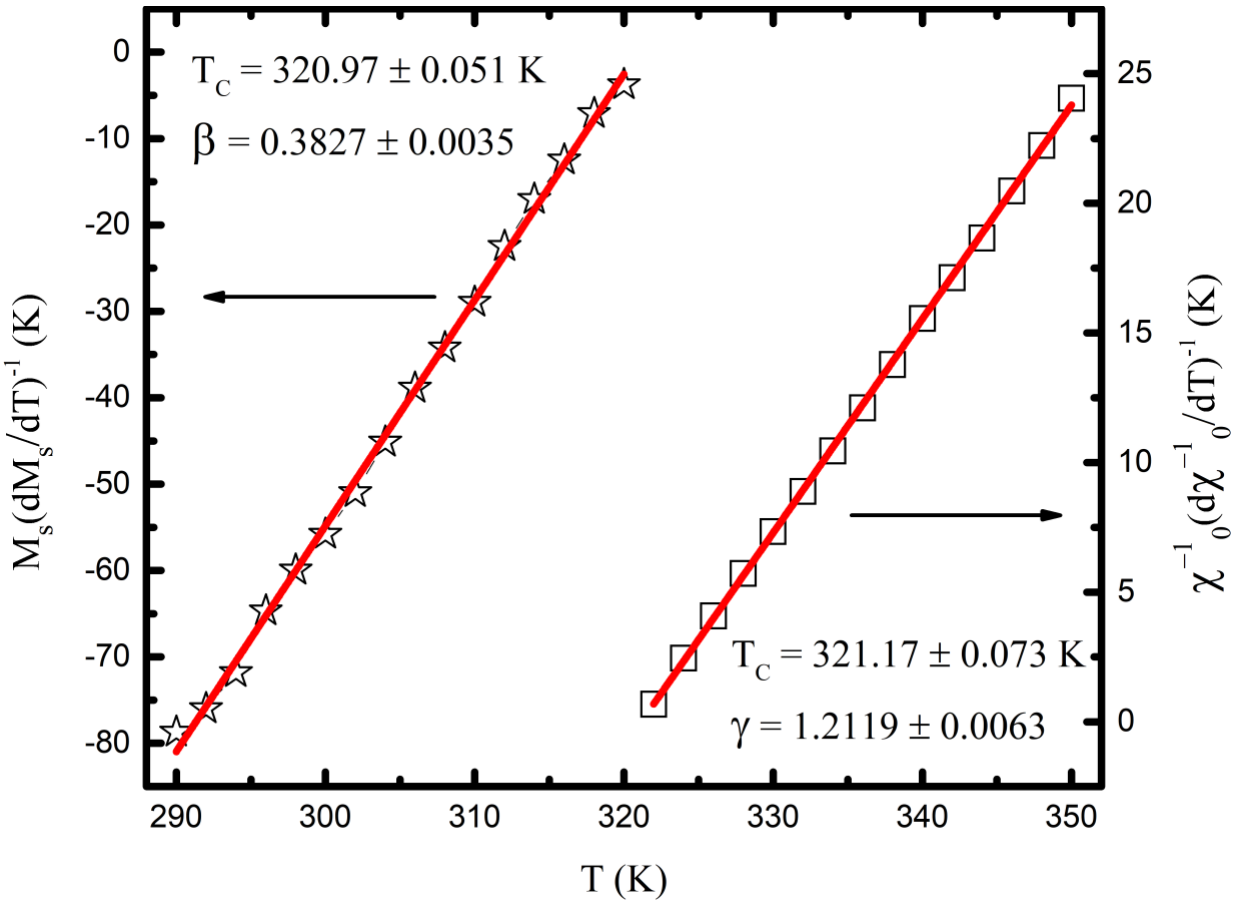

Figure 9: The Kouvel-Fisher plot shows the temperature dependencies of $M_s(T)/[dM_s(T)/dT]^{-1}$ (star symbol) and $\chi_0^{-1}(T)/[d\chi_0^{-1}(T)/dT]$ (squares) for Cr_3Te_4 sample. The best estimated β, γ, and T_C values are indicated in the figure.

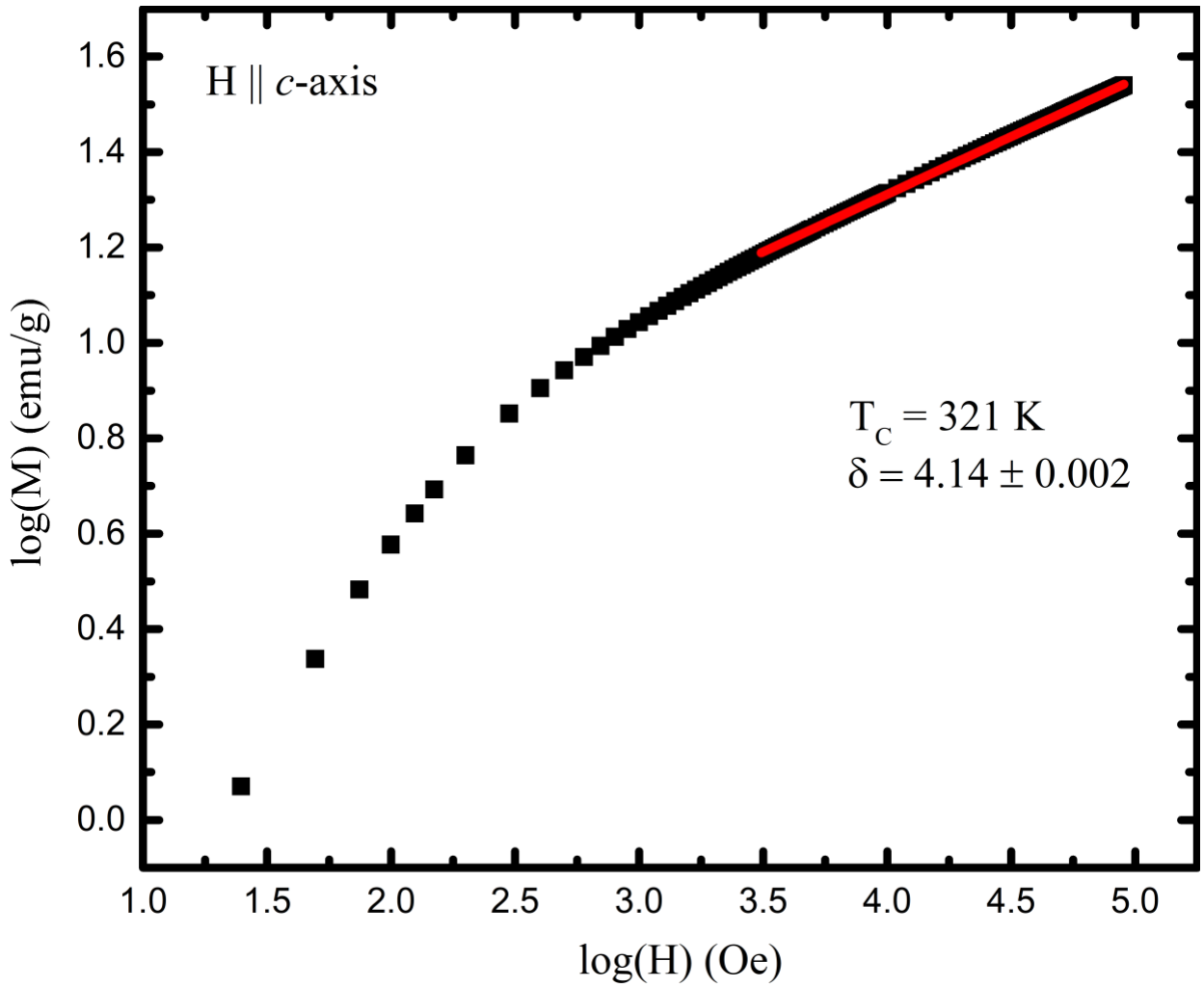

Figure 10: The isothermal magnetization at T_C = 321 K along the *c*-axis of the Cr_3Te_4 crystal gives an estimated $\delta = 4.14$.

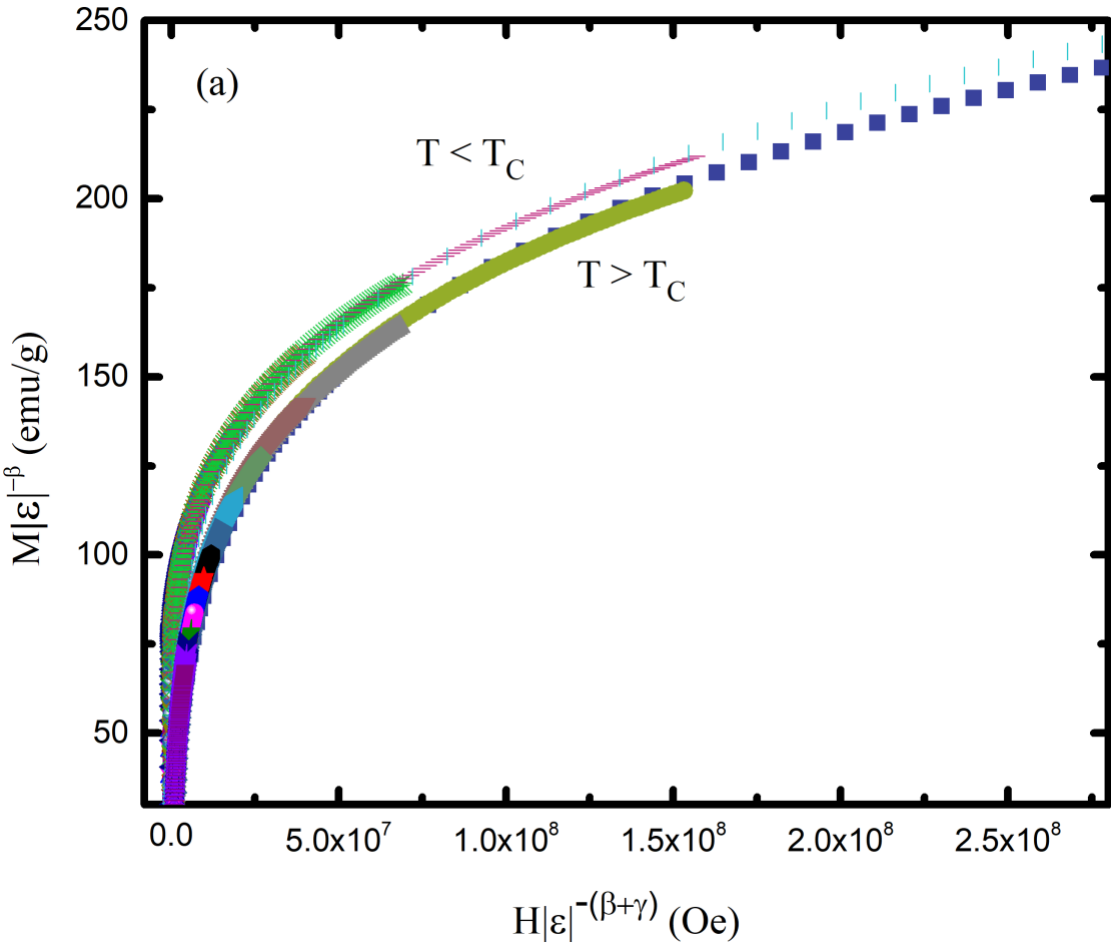
(a)
T < T_C
T > T_C
250
200
150
100
50
0.0
5.0x10^7
1.0x10^8
1.5x10^8
2.0x10^8
2.5x10^8
M|ε|^-β (emu/g)
H|ε|^-(β+γ) (Oe)

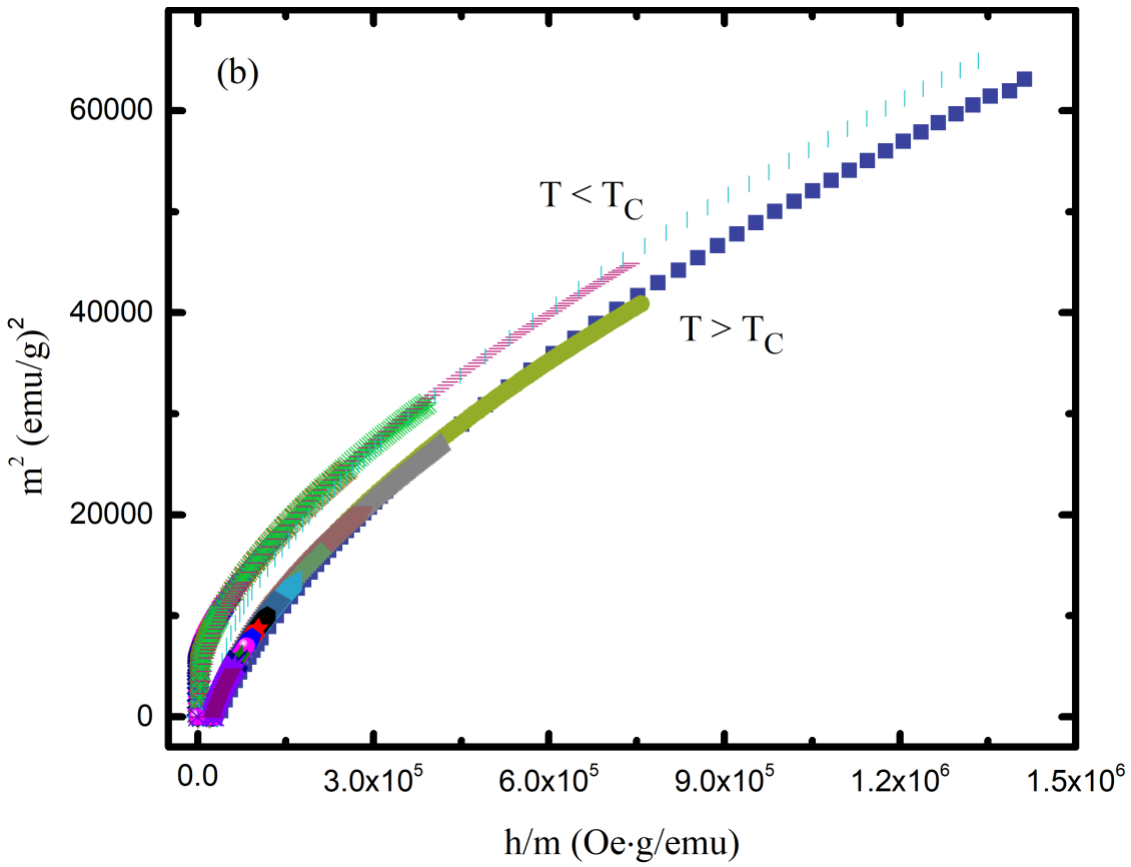
(b)
60000
40000
20000
0
m^2 (emu/g)^2
T < T_C
T > T_C
0.0
3.0x10^5
6.0x10^5
9.0x10^5
1.2x10^6
1.5x10^6
h/m (Oe·g/emu)

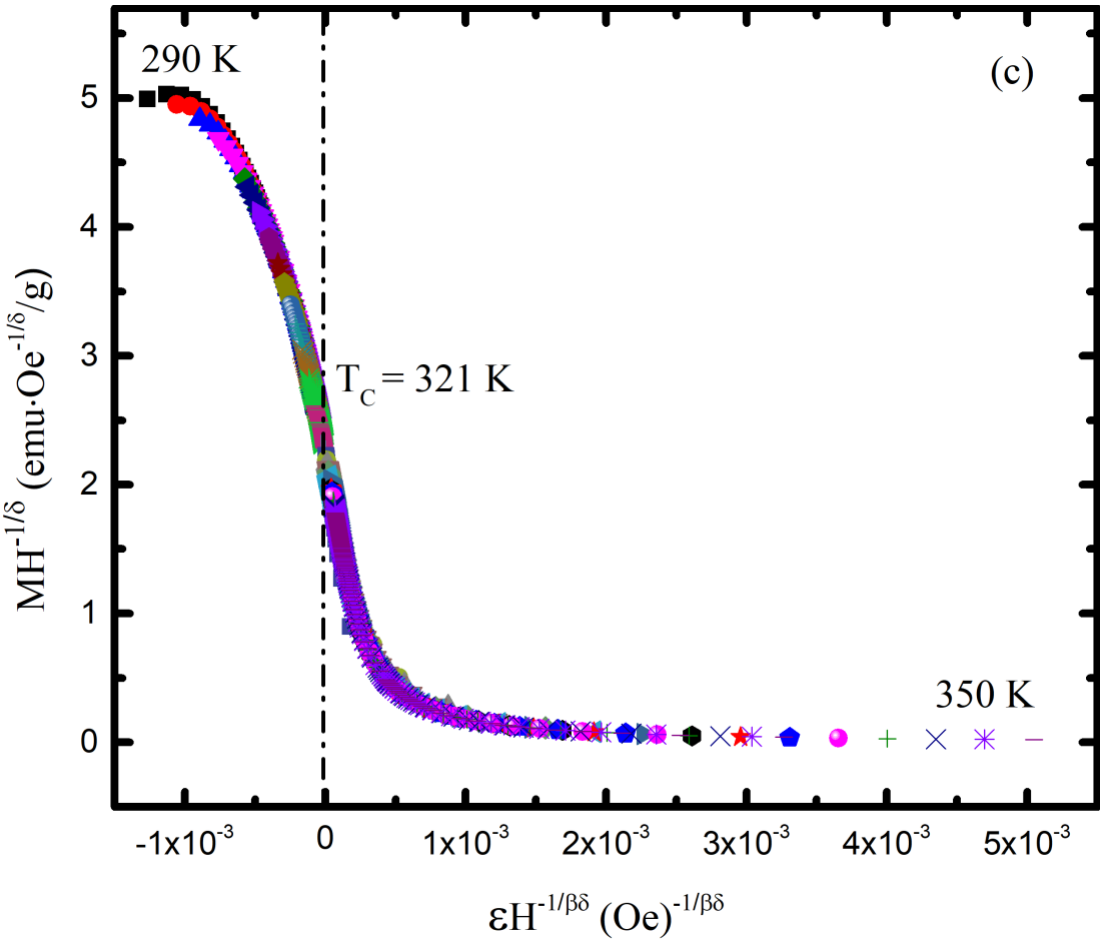

Figure 11: Verification of reliability of our analysis of critical exponents: (a) A plot of normalized magnetization ($m = M|\varepsilon|^{-\beta}$) as a function of normalized field ($h = H|\varepsilon|^{-(\beta+\gamma)}$) of isothermal magnetizations scale into two groups: one below and another above the T_C. This plot shows the accuracy of our critical exponent analysis. (b) The normalized magnetization (m^2) as a function of normalized inverse magnetic susceptibility (h/m) for different temperatures also scales into two groups validating our analysis of critical exponents. (c) All temperature-dependent isothermal magnetization M(H) data maps onto one curve when they are plotted as $MH^{-1/\delta}$ vs. $\varepsilon H^{-1/\beta\gamma}$. These three figures show the reliability of our analysis of critical exponents.

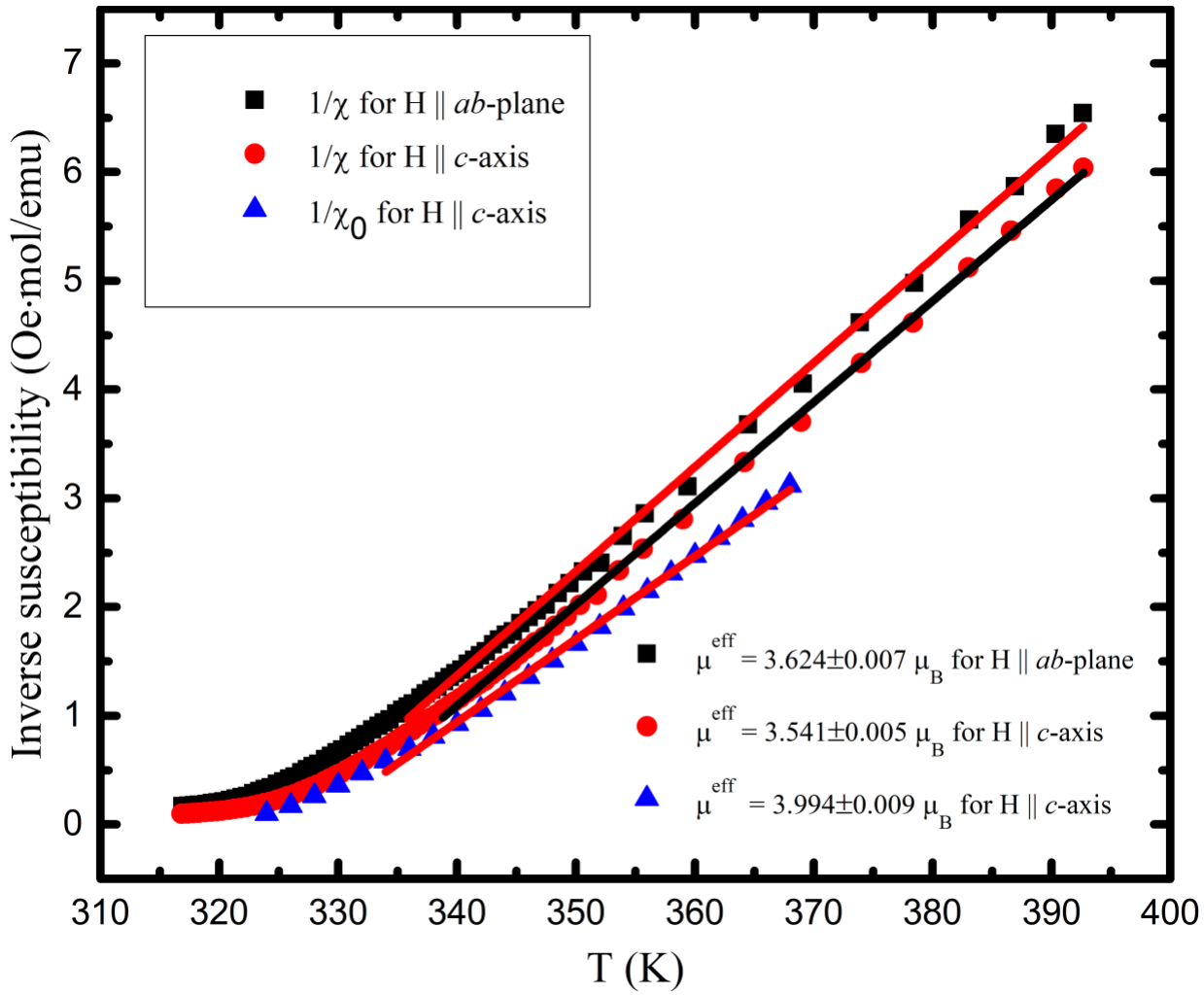

Figure 12: Temperature-dependent inverse magnetic susceptibility along the *c*-axis, *ab*-plane, and inverse initial magnetic susceptibility plots of Cr_3Te_4 sample give effective magnetic moment of 3.624 (±0.007) μ_B, 3.541(±0.005) μ_B, and 3.994 (±0.009) μ_B per Cr atom, respectively.

Table III: This table summarizes estimated critical exponent values of Cr_3Te_4 (this work), five models, and other known Cr-Te binary phases.

Composition	Technique	β	γ	δ
Cr_3Te_4 (this work)	Modified Arrott Plot	0.3814±0.0046	1.2243±0.0036	4.21
Cr_3Te_4 (this work)	Kouvel-Fisher Method	0.3827±0.0035	1.2119±0.0063	4.16
Cr_3Te_4 (this work)	Isothermal Magnetization at T_C = 321 K			4.140±0.002
Theory [50]	Mean Field Model	0.5	1	3
Theory [60]	3D Ising Model	0.325	1.24	4.80
Theory [60]	3D Heisenberg Model	0.365	1.386	4.82
Theory [59]	3D XY Model	0.345	1.361	4.81
Theory [60]	Tricritical Mean Field Model	0.25	1	5
Cr_4Te_5 [23]	Kouvel-Fisher Method	0.387	1.287	4.32
Cr_5Te_8 [61]	Kouvel-Fisher Method	0.321	1.27	4.9
$Cr_{0.62}Te$ [26]	Kouvel-Fisher Method	0.315	1.81	6.75
Cr_5Te_6 [62]	Kouvel-Fisher Method	0.406	1.199	3.95

*Calculated by Widom scaling law: $\delta = 1 + \gamma/\beta$.

Reference:

[1] S. Siddique, C. Chowde Gowda, S. Demiss, R. Tromer, S. Paul, K. K. Sadasivuni, E. F. Olu, A. Chandra, V. Kochat, D. S. Galvão, P. Kumbhakar, R. Mishra, P. M. Ajayan, and C. Sekhar Tiwary *Emerging Two-Dimensional Tellurides*, Materials Today, **51**, 402-426, (2021).

[2] X. Zhang, B. Wang, Y. Guo, Y. Zhang, Y. Chen, and J. Wang, *High Curie Temperature and Intrinsic Ferromagnetic Half-Metallicity in Two-Dimensional Cr_3X_4 (X = S, Se, Te) Nanosheets*, Nanoscale Horiz **4**, 859 (2019).

[3] T. Pramanik, A. Roy, R. Dey, A. Rai, S. Guchhait, H. C. P. Movva, C. C. Hsieh, and S. K. Banerjee, *Angular Dependence of Magnetization Reversal in Epitaxial Chromium Telluride Thin Films with Perpendicular Magnetic Anisotropy*, J Magn Magn Mater **437**, 72 (2017).

[4] A. Roy, S. Guchhait, R. Dey, T. Pramanik, C. C. Hsieh, A. Rai, and S. K. Banerjee, *Perpendicular Magnetic Anisotropy and Spin Glass-like Behavior in Molecular Beam Epitaxy Grown Chromium Telluride Thin Films*, ACS Nano **9**, 3772 (2015).

[5] A. Roy, R. Dey, T. Pramanik, A. Rai, R. Schalip, S. Majumder, S. Guchhait, and S. K. Banerjee, *Structural and Magnetic Properties of Molecular Beam Epitaxy Grown Chromium Selenide Thin Films*, Phys Rev Mater **4**, 025001 (2020).

[6] Y. Wen, Z. Liu, Y. Zhang, C. Xia, B. Zhai, X. Zhang, G. Zhai, C. Shen, P. He, R. Cheng, L. Yin, Y. Yao, M. Getaye Sendeku, Z. Wang, X. Ye, C. Liu, C. Jiang, C. Shan, Y. Long, and J. He, *Tunable Room-Temperature Ferromagnetism in Two-Dimensional Cr_2Te_3*, Nano Lett **20**, 3130 (2020).

[7] J Dijkstra, H H Weitering, C F van Bruggen, C Haas, and R A de Groot, *Band-Structure Calculations, and Magnetic and Transport Properties of Ferromagnetic Chromium Tellurides (CrTe, Cr_3Te_4, Cr_2Te_3)*, Journal of Physics: Condensed Matter **1**, 9141 (1989).

[8] A. F. Andresen, E. Zeppezauer, T. Boive, B. Nordström, and C. I. Brändén, *The Magnetic Structure of Cr_2Te_3, Cr_3Te_4, and Cr_5Te_6*, Acta Chem Scand **24**, 3495 (1970).

[9] G. Chattopadhyay, *The Cr-Te (Chromium-Tellurium) System*, Journal of Phase Equilibria **15**, 431 (1994).

[10] T. Hirone and S. Chiba, *On the Magnetic Anisotropy of Single Crystal of Chromium Telluride*, J Physical Soc Japan **15**, 1991 (1960).

[11] H. Ipser, K. L. Komarek, and K. O. Klepp, *Transition Metal-Chalcogen Systems Viii: The Cr-Te Phase Diagram*, Journal of the Less Common Metals **92**, 265 (1983).

[12] Y. Zhu, X. Kong, T. D. Rhone, and H. Guo, *Systematic Search for Two-Dimensional Ferromagnetic Materials*, Phys Rev Mater **2**, 81001 (2018).

[13] H. Sato, M. Koyama, K. Takada, H. Okuda, K. Shimada, Y. Ueda, J. Ghijsen, and M. Taniguchi, *Electronic Structure of Chromium Chalcogenides*, J Electron Spectros Relat Phenomena **88–91**, 333 (1998).

[14] T. Eto, M. Ishizuka, S. Endo, T. Kanomata, and T. Kikegawa, *Pressure-Induced Structural Phase Transition in a Ferromagnet CrTe*, J Alloys Compd **315**, 16 (2001).

[15] N. Abuawwad, M. dos Santos Dias, H. Abusara, and S. Lounis, *Noncollinear Magnetism in Two-Dimensional $CrTe_2$*, Journal of Physics: Condensed Matter **34**, 454001 (2022).

[16] D. C. Freitas, R. Weht, A. Sulpice, G. Remenyi, P. Strobel, F. Gay, J. Marcus, and M. Núñez-Regueiro, *Ferromagnetism in Layered Metastable 1T-$CrTe_2$*, Journal of Physics: Condensed Matter **27**, 176002 (2015).

[17] X. Zhang, Q. Lu, W. Liu, W. Niu, J. Sun, J. Cook, M. Vaninger, P. F. Miceli, D. J. Singh, S.-W. Lian, T.-R. Chang, X. He, J. Du, L. He, R. Zhang, G. Bian, and Y. Xu, *Room-Temperature Intrinsic Ferromagnetism in Epitaxial $CrTe_2$ Ultrathin Films*, Nat Commun **12**, 2492 (2021).

[18] T. Hamasaki, T. Hashimoto, Y. Yamaguchi, and H. Watanabe, *Neutron Diffraction Study of Cr_2Te_3 Single Crystal*, Solid State Commun **16**, 895 (1975).

[19] S. J. Youn, S. K. Kwon, and B. I. Min, *Correlation Effect and Magnetic Moments in Cr_2Te_3*, J Appl Phys **101**, 09G522 (2007).

[20] F. Wang, J. Du, F. Sun, R. F. Sabirianov, N. Al-Aqtash, D. Sengupta, H. Zeng, and X. Xu, *Ferromagnetic Cr_2Te_3 Nanorods with Ultrahigh Coercivity*, Nanoscale **10**, 11028 (2018).

[21] M. Yamaguchi and T. Hashimoto, *Magnetic Properties of Cr_3Te_4 in Ferromagnetic Region*, J Physical Soc Japan **32**, 635 (1972).

[22] Y. Wang, S. Kajihara, H. Matsuoka, B. K. Saika, K. Yamagami, Y. Takeda, H. Wadati, K. Ishizaka, Y. Iwasa, and M. Nakano, *Layer-Number-Independent Two-Dimensional Ferromagnetism in Cr_3Te_4*, Nano Lett **22**, 9964 (2022).

[23] L.-Z. Zhang, A.-L. Zhang, X.-D. He, X.-W. Ben, Q.-L. Xiao, W.-L. Lu, F. Chen, Z. Feng, S. Cao, J. Zhang, and J.-Y. Ge, *Critical Behavior and Magnetocaloric Effect of the Quasi-Two-Dimensional Room-Temperature Ferromagnet Cr_4Te_5*, Phys Rev B **101**, 214413 (2020).

[24] X. Zhang, T. Yu, Q. Xue, M. Lei, and R. Jiao, *Critical Behavior and Magnetocaloric Effect in Monoclinic Cr_5Te_8*, J Alloys Compd **750**, 798 (2018).

[25] R. Mondal, R. Kulkarni, and A. Thamizhavel, *Anisotropic Magnetic Properties and Critical Behaviour Studies of Trigonal Cr_5Te_8 Single Crystal*, J Mag. Magn Mater **483**, 27 (2019).

[26] Y. Liu and C. Petrovic, *Critical Behavior of the Quasi-Two-Dimensional Weak Itinerant Ferromagnet Trigonal Chromium Telluride $Cr_{0.62}Te$*, Phys Rev B **96**, 134410 (2017).

[27] K. Yaji, A. Kimura, C. Hirai, M. Taniguchi, M. Koyama, H. Sato, K. Shimada, A. Tanaka, T. Muro, S. Imada, and S. Suga, *Electronic Structure of $Cr_{(1-x)}Te$ Studied by Cr 2p Soft x-Ray Magnetic Circular Dichroism*, Phys Rev B **70**, 64402 (2004).

[28] E. F. Bertaut, G. Roult, R. Aleonard, R. Pauthenet, M. Chevreton, and R. Jansen, *Structures Magnétiques de Cr_3X_4 (X = S, Se, Te)*, J. Phys. France **25**, 582 (1964).

[29] B. Hessen, T. M. Siegrist, T. Palstra, S. M. Tanzler, and M. L. Steigerwald, *$Cr_6Te_8(PEt_3)_6$ and a Molecule-Based Synthesis of Cr_3Te_4*, Inorg Chem **32**, 5165 (1993).

[30] K. Yaji, A. Kimura, M. Koyama, C. Hirai, H. Sato, K. Shimada, A. Tanaka, and M. Taniguchi, *Soft X-Ray Magnetic Circular Dichroism Study of Cr Tellurides*, J Appl Phys **97**, 10A316 (2005).

[31] Y. Liu and C. Petrovic, *Anomalous Hall Effect in the Trigonal Cr_5Te_8 Single Crystal*, Phys Rev B **98**, 195122 (2018).

[32] F. Grønvold and E. F. Westrum Jr., *Thermodynamic Aspects of the Magnetic Transitions in the Chromium Tellurides Heat Capacities of Cr_5Te_6, Cr_3Te_4 and Cr_2Te_3 from 5 to 350°K*, Z Anorg Allg Chem **328**, 272 (1964).

[33] K. Sato, Y. Aman, M. Hirai, and M. Fujisawa, *Reflectivity Spectra in Single Crystals of Cr_3Te_4, Cr_2Te_3 and Cr_2Se_3 between 0.3 and 23 EV*, J Physical Soc Japan **59**, 435 (1990).

[34] K. Sato, Y. Aman, and M. Hirai, *MAGNETO-OPTICAL EFFECT IN A SINGLE CRYSTAL OF Cr_3Te_4*, Le Journal de Physique Colloques **49**, C8 (1988).

[35] W. Liu, Y. Dai, Y.-E. Yang, J. Fan, L. Pi, L. Zhang, and Y. Zhang, *Critical Behavior of the Single-Crystalline van Der Waals Bonded Ferromagnet $Cr_2Ge_2Te_6$*, Phys Rev B **98**, 214420 (2018).

[36] Y. Liu and C. Petrovic, *Anisotropic Magnetocaloric Effect and Critical Behavior in $CrCl_3$*, Phys Rev B **102**, 14424 (2020).

[37] Y. Liu, Z. Hu, and C. Petrovic, *Anisotropic Magnetocaloric Effect and Critical Behavior in $CrSbSe_3$*, Phys Rev B **102**, 14425 (2020).

[38] J. Yan X. Luo, F. C. Chen, J. J. Gao, Z. Z. Jiang, G. C. Zhao, Y. Sun, H. Y. Lv, S. J. Tian, Q. W. Yin, H. C. Lei, W. J. Lu, P. Tong, W. H. Song, X. B. Zhu, and Y. P. Sun *Anisotropic Magnetic Entropy Change in the Hard Ferromagnetic Semiconductor VI_3*, Phys Rev B **100**, 94402 (2019).

[39] V. Franco, J. S. Blázquez, B. Ingale, and A. Conde, *The Magnetocaloric Effect and Magnetic Refrigeration Near Room Temperature: Materials and Models*, Annu Rev Mater Res **42**, 305 (2012).

[40] V. Franco, A. Conde, J. M. Romero-Enrique, and J. S. Blázquez, *A Universal Curve for the Magnetocaloric Effect: An Analysis Based on Scaling Relations*, Journal of Physics: Condensed Matter **20**, 285207 (2008).

[41] H. Oesterreicher and F. T. Parker, *Magnetic Cooling near Curie Temperatures above 300 K*, J Appl Phys **55**, 4334 (1984).

[42] V. Chaudhary, X. Chen, and R. V Ramanujan, *Iron and Manganese Based Magnetocaloric Materials for near Room Temperature Thermal Management*, Prog Mater Sci **100**, 64 (2019).

[43] J. Kieffer, V. Valls, N. Blanc, and C. Hennig, *New Tools for Calibrating Diffraction Setups*, J Synchrotron Radiat **27**, 558 (2020).

[44] B. H. Toby and R. B. Von Dreele, *GSAS-II: The Genesis of a Modern Open-Source All Purpose Crystallography Software Package*, J Appl Crystallogr **46**, 544 (2013).

[45] M. Sharma and D. Mishra, *CrysX: Crystallographic Tools for the Android Platform*, J Appl Crystallogr **52**, 1449 (2019).

[46] See Supplemental Material at [link to be inserted by the publisher] for the crystallographic information file (cif) of our Cr_3Te_4 sample.

[47] Y. Liu, M. Abeykoon, E. Stavitski, K. Attenkofer, and C. Petrovic, *Magnetic Anisotropy and Entropy Change in Trigonal Cr_5Te_8*, Phys Rev B **100**, 245114 (2019).

[48] *Introduction to Phase Transitions and Critical Phenomena. By H. Eugene Stanley, Oxford University Press, Oxford, 1987*, Int J Quantum Chem **35**, 583 (1989).

[49] A. Arrott and J. E. Noakes, *Approximate Equation of State For Nickel Near Its Critical Temperature*, Phys Rev Lett **19**, 786 (1967).

[50] A. Arrott, *Criterion for Ferromagnetism from Observations of Magnetic Isotherms*, Physical Review **108**, 1394 (1957).

[51] S.K. Banerjee, *On a Generalised Approach to First and Second Order Magnetic Transitions*, Physics Letters **12**, 16 (1964).

[52] M E Fisher, *The Theory of Equilibrium Critical Phenomena*, Reports on Progress in Physics **30**, 615 (1967).

[53] F. K. Lotgering and E. W. Gorter, *Solid Solutions between Ferromagnetic and Antiferromagnetic Compounds with NiAs Structure*, Journal of Physics and Chemistry of Solids **3**, 238 (1957).

[54] [54] A. K. Pramanik and A. Banerjee, *Critical Behavior at Paramagnetic to Ferromagnetic Phase Transition in $Pr_{0.5}Sr_{0.5}MnO_3$: A Bulk Magnetization Study*, Phys Rev B **79**, 214426 (2009).

[55] J. S. Kouvel and M. E. Fisher, *Detailed Magnetic Behavior of Nickel Near Its Curie Point*, Physical Review **136**, A1626 (1964).

[56] B. Widom, *Equation of State in the Neighborhood of the Critical Point*, J Chem Phys **43**, 3898 (2004).

[57] M. E. Fisher, S. Ma, and B. G. Nickel, *Critical Exponents for Long-Range Interactions*, Phys Rev Lett **29**, 917 (1972).

[58] S. F. Fischer, S. N. Kaul, and H. Kronmüller, *Critical Magnetic Properties of Disordered Polycrystalline Cr_{75} Fe_{25} and $Cr_{70}Fe_{30}$ Alloys*, Phys Rev B **65**, 64443 (2002).

[59] S. N. Kaul, *Static Critical Phenomena in Ferromagnets with Quenched Disorder*, J Magn Magn Mater **53**, 5 (1985).

[60] D. Kim, B. Revaz, B. L. Zink, F. Hellman, J. J. Rhyne, and J. F. Mitchell, *Tricritical Point and the Doping Dependence of the Order of the Ferromagnetic Phase Transition of La_{1-x}Ca_{x}MnO_{3}*, Phys Rev Lett **89**, 227202 (2002).

[61] X. Zhang, T. Yu, Q. Xue, M. Lei, and R. Jiao, *Critical Behavior and Magnetocaloric Effect in Monoclinic Cr_5Te_8* , J Alloys Compd **750**, 798 (2018).

[62] L.-Z. Zhang, Q.-L. Xiao, F. Chen, Z. Feng, S. Cao, J. Zhang, and J.-Y. Ge, *Multiple Magnetic Phase Transitions and Critical Behavior in Single Crystal Cr_5Te_6*, J Magn Magn Mater **546**, 168770 (2022).